Carbon-supported PdM (M = Au and Sn) nanocatalysts for the electrooxidation of ethanol in high pH media

Qinggang He[a], Wei Chen[b], Sanjeev Mukerjee[a,*], Shaowei Chen[b,**], František Laufek[c]

[a] Department of Chemistry and Chemical Biology, Northeastern University, 360 Huntington Avenue, Boston, MA 02115, United States
[b] Department of Chemistry and Biochemistry, University of California, 1156 High Street, Santa Cruz, CA 95064, United States
[c] Czech Geological Survey, Czech Republic

ARTICLE INFO

ABSTRACT

Carbon-supported Pd_4Au- and $Pd_{2.5}Sn$-alloyed nanoparticles were prepared by a chemical reduction method, and characterized by a wide array of experimental techniques including mass spectrometry, transmission electron microscopy, and X-ray diffraction spectroscopy. Ethanol electrooxidation on the as-synthesized catalysts and commercial Pt/C was then investigated and compared in alkaline media by cyclic voltammetry, chronoamperometry, and electrochemical impedance spectroscopy studies at room temperature. Voltammetric and chronoamperometric measurements showed higher current density and longer term stability in ethanol oxidation with the palladium alloy nanocatalysts than with the commercial one. Electrochemical impedance spectroscopy and Tafel plots were employed to examine the charge-transfer kinetics of ethanol electrooxidation. The results suggest that whereas the reaction kinetics might be somewhat more sluggish on the Pd-based alloy catalysts than on commercial Pt/C, the former appeared to have a higher tolerance to surface poisoning. Overall, the Pd-based alloy catalysts represent promising candidates for the electrocatalytic oxidation of ethanol, and Pd_4Au/C displays the best catalytic activity among the series for the ethanol oxidation in alkaline media.

1. Introduction

Recently, anion exchange membrane fuel cells (AEMFCs) have revitalized alkaline fuel-cell technology. AEMFCs involve the replacement of conventional liquid electrolytes with an alkaline anion exchange membrane to prevent the precipitation of carbonates (CO_3^{2-}/HCO_3^-) [1,2], and exhibit several intrinsic advantages as compared to the acidic counterparts: more facile electrocatalytic reaction dynamics, the possibility of using inexpensive non-noble electrocatalysts, wider choices of fuel feeds, better water management, and no need of expensive fluorinated polymers. Of these, methanol has been examined extensively as a promising fuel candidate. However, the feasible application of methanol is hindered by its toxicity and potential pollution to the environment. Ethanol on the other hand, is environmentally friendly, and may serve as a potential alternative because it has a higher energy density than methanol [3]. In addition, ethanol can be produced through a green fermentation process that makes it less dependent on fossil fuels.

Pt-based binary or ternary alloy (nano)materials (e.g., PtRu and PtSn) have been recognized as the state-of-the-art anodic electro-

catalysts for DEFCs [4–6]. However, strong motivation remains in the pursuit of non-Pt catalysts due to the limited availability and high price of Pt [7,8]. A number of catalysts have been prepared and examined for the electrooxidation of ethanol, particularly in alkaline media. For instance, Pd and Ru have been used as a replacement for Pt-based catalysts in the electrooxidation of ethanol [8–12]. These materials have shown marked superiority compared to Pt in terms of reactivity, poison tolerance, and cost. Substantial research efforts have also been devoted to the systematic manipulation of the catalyst composition and structure for further improvement of the catalytic performance. Wang et al. [12] and Xu et al. [13] prepared Pd nanowire arrays by a template-electrodeposition method and observed a twofold enhancement of the voltammetric peak current, along with a slow decay of the voltammetric current, in ethanol oxidation in comparison to that of commercial PtRu/C catalysts. In other studies, the influence of the catalyst support on the activity of Pd for ethanol oxidation was evaluated [11,14–16]. For example, carbon microspheres have been used to support Pd electrocatalyst [9,14], which displayed better performance than Pt deposited on carbon black as a consequence of the synergistic interactions between Pd and the carbon substrate. Xu et al. [17,18], Hu et al. [19], and Shen and Xu [8] investigated the activities of oxide-promoted Pd/C electrocatalysts for ethanol electrooxidation in alkaline media by cyclic voltammetry and chronopotentiometry. Such electrocatalysts showed orders of magnitude enhancement in

* Corresponding author.
** Corresponding author. Tel.: +1 8314595841; fax: +1 8314592935.
E-mail address: schen@chemistry.ucsc.edu (S. Chen).

activities and good steady-state behaviors for ethanol oxidation. The authors argued that the oxide functions were analogous to those of Ru in PtRu [20–22] and SnO in PtSnO catalysts [23], where the oxides facilitated the conversion of CO-like poisoning species on the Pd surface to CO_2 at lower potentials. Another postulation is that the oxides may have sufficient electron affinity to help break the C–C bond, as SnO does in PtSnO and PtSnInO catalysts.

Despite the substantial progress, much remains to be done, particularly in the search of effective of Pd-based alloys in the oxidation of ethanol. In this paper we prepared two alloy nanoparticles, Pd_4Au and $Pd_{2.5}Sn$, and compared their electrocatalytic activity in ethanol oxidation to commercial Pt/C catalysts. Electrochemical investigations (cyclic voltammetry, chronoamperometry, and electrochemical impedance spectroscopy (EIS)) show that the as-prepared alloy particles exhibit a somewhat larger peak current density and slower current decay than commercial Pt/C catalysts, suggesting that they might serve as promising candidates in the direct oxidation of ethanol.

2. Experimental

Unless otherwise stated, all chemicals were ACS reagent grade and used as received. Palladium chloride ($PdCl_2$), gold chloride ($AuCl_3$), tin acetate ($SnAc_2$), citrate acid, sodium borohydride ($NaBH_4$), and dihydrogen hexachloroplatinate (IV) hydrate ($H_2PtCl_6 \cdot xH_2O$) were obtained from Sigma–Aldrich. Vulcan carbon was dried at $100\,°C$ in a high vacuum oven prior to use. Commercially available catalysts of 30 wt% platinum supported on Vulcan XC72 were obtained from E-TEK.

To make PdAu/C nanoparticles, 200 mg of carbon was dispersed by sonication for 30 min in a $0.2\,mol\,L^{-1}$ citrate acid solution. A calculated amount of a mixture of $0.1\,mol\,L^{-1}$ $PdCl_2$ and $AuCl_3$ was added into the above solution under magnetic stirring. The atomic ratio of Pd to Au was kept at 4:1 and the combined metal loading on carbon was 30%. In the case of PdSn/C catalysts, the atomic ratio of Pt to Sn was kept at 3:1 and the total metal loading was also 30%. After the temperature of the slurry was increased to $60\,°C$, $NaBH_4$ was slowly added in excess and the solution was stirred for another 4 h. The resulting precipitate was washed with a copious amount of water and dried at $80\,°C$ overnight. The compositions of the catalysts were then analyzed by VG Elemental Plasmaquad-2 (PQ2) ICP-MS. The results are summarized in Table 1, where the resulting particles exhibited a composition of Pd_4Au/C and $Pd_{2.5}Sn/C$, very close to the initial respective feed ratio used in the preparation.

Powder X-ray diffraction (XRD) patterns of the catalysts were acquired using a Rigaku X-ray diffractometer with Cu Kα radiation. The particle size of the dispersed metal crystallites was estimated from the broadening of the diffraction peaks using the Debye–Scherrer formula. The morphology and particle size distribution of the as-synthesized catalysts were examined with a JEOL JEM-1000 transmission electron microscope (TEM).

All electrochemical measurements were carried out at room temperature in a standard three-compartment electrochemical cell using a rotating ring-disk electrode setup from Pine Instruments connected to an Autolab (Ecochemie Inc., model-PGSTAT 30) potentiostat. All potentials were measured with respect to a sealed hydrogen reference electrode (RHE) made from the same concentration of the electrolyte used in the experiment. The catalysts were loaded onto a glassy carbon electrode (diameter 5 mm) at a surface density of $15\,\mu g\,cm^{-2}$ of noble metals for voltammetric measurements. The instantaneous current (j_0) during ethanol oxidation was measured by potential step techniques or short chronoamperometric measurements to evaluate the kinetic parameters [24]. Specifically, the electrode potential was oscillated between the low and high potential limits for two cycles. The lower potential was set at 0 V at the hydrogen UPD region, and the upper potential was set at +1.05 V where residues of adsorbed species on the electrode surface would be removed. The potential was then set to a desired value for current transient measurements. EIS measurements were carried out using an EG&G PARC Potentiostat/Galvanostat model 283 and Frequency Response Detector (model 1025). The impedance spectra were recorded between 100 kHz and 10 mHz with the amplitude (rms value) of the ac signal at 10 mV.

3. Results and discussion

The structures of the Pd_4Au/C and $Pd_{2.5}Sn/C$ nanoparticle catalysts were first characterized by XRD and TEM studies. From the XRD patterns depicted in Fig. 1, it can be seen that the diffraction peaks for Pd(1 1 1), (2 0 0), and (2 2 0) are very well-defined, as is C(0 0 2) of the supporting matrix. For the Pd_4Au/C sample (dashed curve), a series of diffraction peaks can be indexed to gold crystalline planes such as Au(1 1 1), (2 0 0), and (2 2 0); the XRD pattern of $Pd_{2.5}Sn/C$ (solid curve) is very similar to that of Pd_3Sn/C in reference to JCPDS files (41-1409), with rather intense peaks for Sn(3 1 1) and (2 2 1). These results suggest that the obtained catalysts were
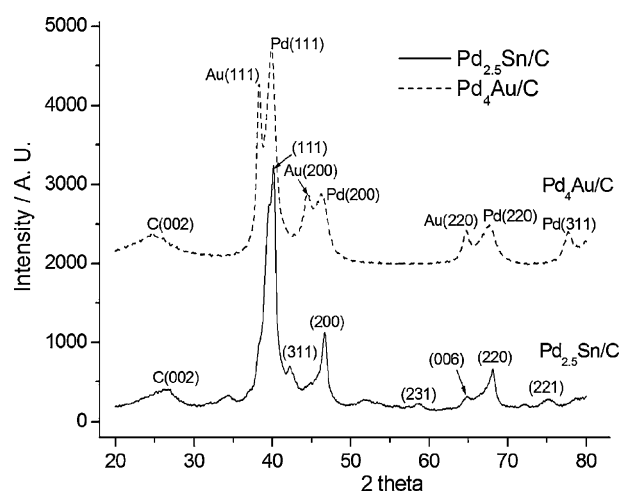
Table 1
Composition of Pd_4Au/C and $Pd_{2.5}Sn/C$ catalysts prepared in-house.

Catalyst	Nominal composition		Composition from ICP analysis	
	Pd wt%	Pd:M (atomic)	Pd wt%	Pd:M (atomic)
Pd_4Au/C	28.7	4:1	27.0	3.89:1
$Pd_{2.5}Sn/C$	29.3	3:1	27.8	2.53: 1

Fig. 1. XRD patterns of Pd_4Au/C (- - -) and $Pd_{2.5}Sn/C$ (—).

Table 2
XRD data of Pd_4Au/C and $Pd_{2.5}Sn/C$ catalysts.

Catalyst	Lattice types	Pt (1 1 1) at 2θ	Crystallite size[a] (nm)	Lattice parameter (Å)	Pd–Pd bond distance (Å)	Space group
Pd_4Au/C	Face centered cubic	39.89	6.5	$a = b = c = 3.91$	2.77	Fm3m
$Pd_{2.5}Sn/C$	Cubic	40.15	7.4	$a = 5.65$, $b = 4.31$, $c = 8.12$	2.46	Pnma

[a] The average crystallite size was calculated using the Debye–Scherrer equation ($Z = C\lambda / B\cos\theta$) [25].
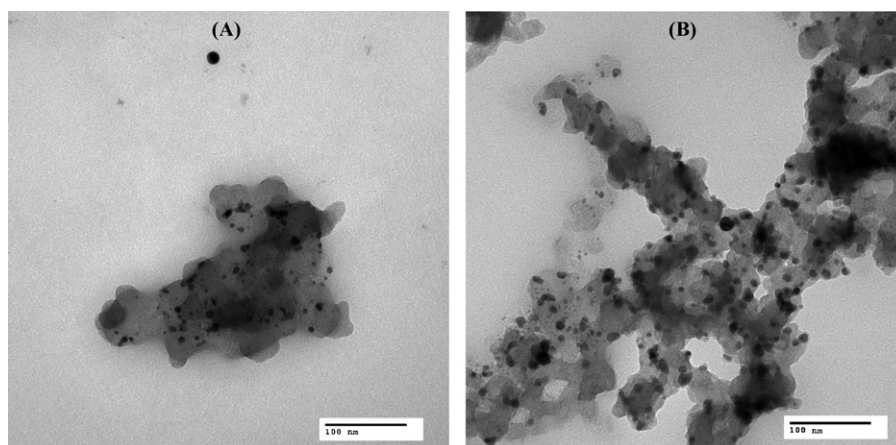
Fig. 2. TEM micrographs of (A) Pd$_4$Au/C and (B) Pd$_{2.5}$Sn/C. Scale bars are 100 nm.

highly crystalline. In addition, based on the crystalline lattice unit cells (Table 2), the Pd$_4$Au/C sample may be ascribed to the cubic crystal system and Fm3m space group with a lattice constant of $a = b = c = 3.91$ Å. In contrast, Pd$_{2.5}$Sn/C appears to be consistent with an orthorhombic crystal system and Pnma space group, with lattice constants of $a = 5.65$ Å, $b = 4.31$ Å, and $c = 8.12$ Å.

Based on the width of the Pd(1 1 1) peak, the size of the nanocrystallites was estimated using the Debye–Scherrer equation [25], which gave values of 6.5 and 7.4 nm, for the Pd$_4$Au/C and Pd$_{2.5}$Sn/C, respectively. These values support the results from the TEM measurements. Fig. 2 shows a representative TEM micrograph of the Pd$_4$Au/C and Pd$_{2.5}$Sn/C samples. The figure shows that in both samples the nanoparticles were very well dispersed on the carbon supports. The average particle size of Pd$_4$Au/C and Pd$_{2.5}$Sn/C was found to be 6.8 and 8.4 nm, respectively. These samples were then subjected to electrochemical assessment of their electrocatalytic activity in ethanol oxidation.

Fig. 3(A) shows the cyclic voltammograms of the Pd$_4$Au/C and Pd$_{2.5}$Sn/C particles, as well as commercial Pt/C catalysts in 0.25 mol L^{-1} KOH, all at a loading of 15 μg cm^{-2} of noble metals on the electrode surface. The geometric area of the glassy carbon electrode (0.196 cm^2) was used in the calculation of current density. All catalysts exhibited similar responses in the double-layer charging region from +0.5 to +0.7 V. However, hydrogen evolution occurred at somewhat more positive potentials on the PdAu/C and PdSn/C electrodes than on the Pt/C electrode, suggesting that hydrogen adsorption might be better facilitated at the Pd-based catalyst surface. The corresponding electrochemical active surface (EAS) area of the catalysts was evaluated by the Coulombic charge associated with hydrogen desorption (Q_H) [12,13], which was indicated by the broad peaks between +0.2 and +0.5 V in the anodic scan [18]. Q_H for Pt/C (0.67 C) was somewhat higher than those for Pd$_4$Au/C (0.244 C) and Pd$_{2.5}$Sn/C (0.242 C), possibly as a consequence of the alloyed morphologies of the PdAu and PdSn particle surfaces.

The voltammetric responses of the catalysts in ethanol oxidation are shown in Fig. 3(B). It can be seen that whereas the anodic onset potential (Pt/C, +0.47 V; Pt$_4$Au/C, +0.50 V; Pt$_{2.5}$Sn/C, +0.53 V) and peak potential (Pt/C, +0.80 V; Pd$_4$Au/C, +0.90 V; Pd$_{2.5}$Sn/C, +0.87 V) for ethanol oxidation appear to be more negative on Pt/C than on Pd$_4$Au/C and Pd$_{2.5}$Sn/C, the current density of the Pd-based catalysts was substantially greater (12 mA cm^{-2} for Pt/C, 20 mA cm^{-2} for Pd$_4$Au/C and Pd$_{2.5}$Sn/C). In comparison to the Pd/C catalysts [17] used previously in ethanol oxidation, the current density observed above with the Pd$_4$Au/C and Pd$_{2.5}$Sn/C electrodes was also significantly higher, suggesting promoting effects of the Au and Sn alloying.

According to the reaction mechanism of ethanol oxidation proposed by Li et al. [26], the adsorbed intermediates are CH$_3$CHOH$_{ads}$ and CH$_3$COOH$_{ads}$ in the low and high potential regions, respectively. However, our previous studies have shown that acetic acid
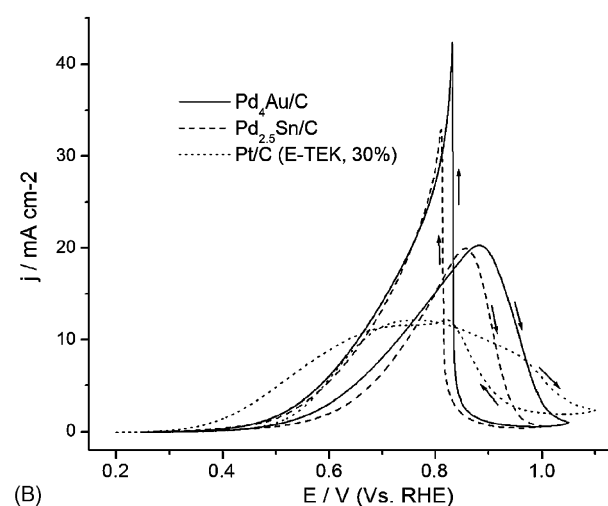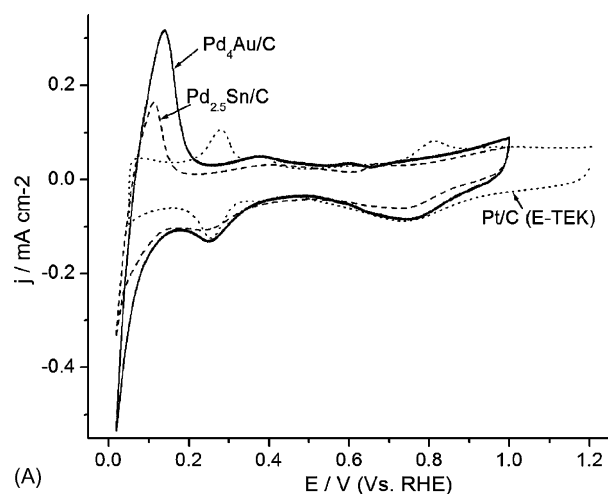

Fig. 3. Cyclic voltammograms of a glassy carbon electrodes modified with Pt/C (E-TEK, 30%, ...), Pd4Au/C (—), and Pd2.5Sn/C (- - -) in (A) 0.25 mol L^{-1} KOH and (B) 0.25 mol L^{-1} KOH + 1 mol L^{-1} ethanol at room temperature. The Pt and Pd loadings were all 15 μg cm^{-2}, and the potential sweep rate was 10 mV s^{-1}.
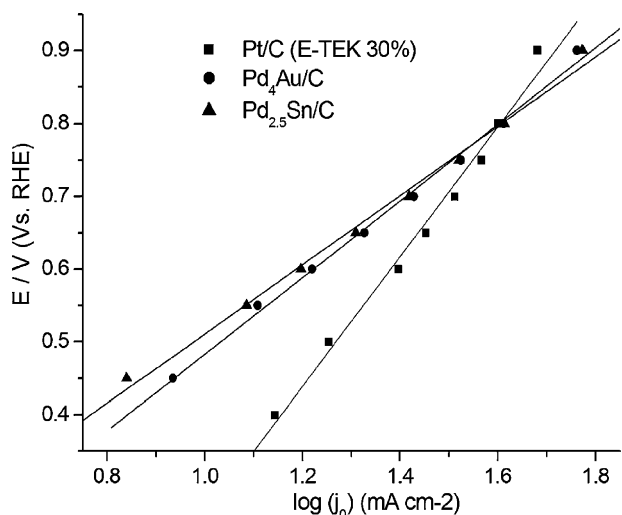
Fig. 4. Semilogarithmic $\log(j_0)$ vs. electrode potential plots for ethanol oxidation on Pt/C (E-TEK 30%), $Pd_{2.5}Sn/C$, and Pd_4Au/C in $0.25\,mol\,L^{-1}$ KOH + $1\,mol\,L^{-1}$ ethanol. Pt and Pd loadings were all $15\,\mu g\,cm^{-2}$.

Fig. 5. Chronoamperometric profiles of Pt/C (E-TEK, 30%), $Pd_{2.5}Sn/C$, and Pd_4Au/C at +0.55 V in $0.25\,mol\,L^{-1}$ KOH + $1\,mol\,L^{-1}$ ethanol. Pt and Pd loadings were all $15\,\mu g\,cm^{-2}$.

was fairly resistant to electrooxidation in basic media [27]. Therefore, the anodic currents observed above in panel (B) are most likely due to the oxidation of acetaldehyde-based intermediates as the electrode potential sweeps anodically, and reach a peak that corresponds to the oxidation of freshly chemisorbed ethanol [14]. At more positive electrode potentials, the oxidation current drops because of Pd oxidation and the associated loss of surface active sites. In the return scan, the Pd active sites are recovered by electroreduction of the Pd oxide species, and the adsorbed intermediates may be converted to acetaldehyde from acetic acid. Consequently, the current peak in the cathodic scan is primarily associated with the oxidative removal of carbonaceous species that were not completely oxidized in the forward scan, in addition to newly adsorbed species from bulk ethanol.

The results observed in panel (B) are in line with kinetic studies that are shown in the Tafel plots (Fig. 4). Tafel plots for electrooxidation of methanol or ethanol have been converted directly from cyclic voltammograms in several studies [8,16,28,29]. However, the voltammetric current in ethanol oxidation may not fully reflect the kinetic current on certain catalysts, since it is typically affected by surface-poisoning ethanolic species. This may include the original ethanol fuel, surface-poisoning species (e.g., linearly adsorbed CO_L and CO_2, $CH_{x,ad}$ species) [30–33], and final products (CO_2, acetaldehyde and acetic acid) [31]. Therefore, fast chronoamperometric techniques have been employed to assess the kinetic current density of the elementary processes involved in ethanol decomposition, by acquiring the instantaneous current of ethanol oxidation within the context of the platinum or palladium surface structure [24]. Fig. 4 shows the Tafel plots (kinetics current as a function of potential) of the ethanol oxidation at the three catalysts, where an appreciable difference of the Tafel slope is evident, suggesting that the mechanism of ethanol oxidation may vary on the Pt and Pd-based catalysts. The mechanism of electrooxidation of ethanol is still controversial and debatable [34–37]. However, it is generally accepted that the first step involves the dissociative adsorption of ethanol on the catalyst surface:

$$Pt + CH_3CH_2OH \rightarrow Pt\text{-adsorbate} + e^- \qquad (1)$$
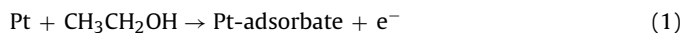
Note that the Gibb's free energy of a reaction is related to the electrochemical potential (E) by the following relationship, $\Delta G = -nFE$. As a result, the onset potential for ethanol oxidation is directly related to the activation energy of the reaction. Previous studies [38–40] have shown that the Fermi level must be changed
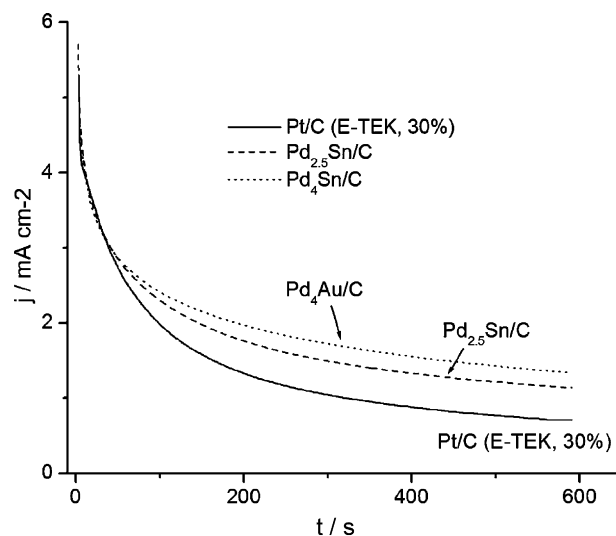
after the formation of metal-oxide species on the Pd surface, resulting in an increase of the activation energy, and hence the larger overpotential and sluggish kinetics for ethanol adsorption on Pd.

Fig. 4 also shows that the instantaneous current appears to decrease in the order of Pt/C $\gg$ PdAu/C > PdSn/C, especially at low electrode potentials; however, at potentials more positive than +0.80 V, the trend reverses, Pt/C < PdAu/C < PdSn/C. The observed discrepancy of the oxidation current at different potentials may be accounted for by the higher activity of Pd to form metal-oxide surface species [38,41–43]. Consequently, more Pt active sites are available for ethanol oxidation at low potentials. Of interest is the observation that peak current density on both Pd_4Au/C and $Pd_{2.5}Sn/C$ is higher than that on Pt/C as depicted in cyclic voltammetric measurements in Fig. 3(B). This suggests that the Pd-based catalysts are less likely to be poisoned and have better stability, which was confirmed by the chronoamperometric test in Fig. 5 (and electrochemical impedance spectroscopy measurements in Figs. 6 and 7). From the long-term current–time curves, current decays more rapidly on Pt/C than on Pd_4Au/C or $Pd_{2.5}Sn/C$, although the initial current on Pt/C is the highest. From the viewpoint of real applications in direct ethanol fuel cells, the as-synthesized Pd_4Au/C and $Pd_{2.5}Sn/C$ appear to be more suitable than commercial Pt/C catalysts because of their superior efficiency.

EIS has been shown to be a sensitive electrochemical technique for the studies of the electrooxidation kinetics of small organic molecules in fuel cells [44,45]. EIS was used in this study to investigate the kinetics of ethanol oxidation on the three kinds of electrodes. Fig. 6(A–C) displays the Nyquist complex-plane impedance spectra of ethanol oxidation on Pt/C, Pd_4Au/C and $Pd_{2.5}Sn/C$ electrodes, respectively, at four representative electrode potentials (+0.35, +0.55, +0.80, and +0.90 V). The measurements were made in $0.25\,mol\,L^{-1}$ KOH + $1\,mol\,L^{-1}$ ethanol, and the electrode potentials were varied from +0.35 to +0.90 V. For ethanol oxidation on the Pt/C electrode (panel A), it is shown that at potentials below +0.55 V, the impedance arcs appear in the second quadrant instead of the conventional first one. Negative impedance behaviors were also observed previously in the electrooxidation of methanol and formic acid on Pt and other Pt-based alloy electrodes, and were usually attributed to the adsorption of reaction intermediates on the catalyst surface [46–49]. It is well known that for fuel oxidation on Pt, there is heavy CO adsorption (poisoning) on the Pt surface. The negative impedance in this work may be attributed to the oxidative removal of CO intermediates because of the
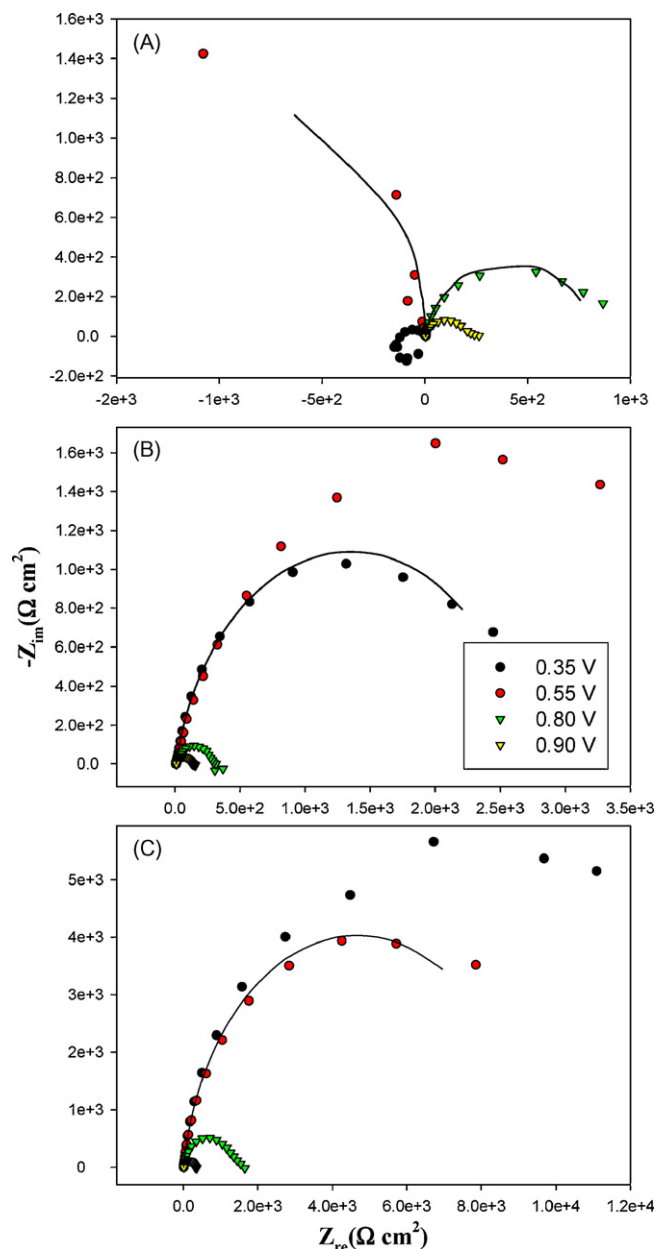
Fig. 6. Complex-plane (Nyquist) impedance plots of the ethanol oxidation on Pt/C (A), Pd$_4$Au/C (B) and Pd$_{2.5}$Sn/C (C) electrodes in 0.25 mol L^{-1} KOH + 1 mol L^{-1} ethanol at different electrode potentials which are shown in the figure legends. Solid lines are representative simulations based on the equivalent circuits shown in Fig. 8.

Fig. 7. Complex-plane (Bode plots) impedance plots of ethanol oxidation on Pt/GC (A), Pd$_4$Au/C (B), and Pd$_{2.5}$Sn/C (C) electrodes in 0.25 mol L^{-1} KOH + 1 mol L^{-1} ethanol at varied electrode potentials.

formation of chemisorbed hydroxyl species in this potential range [15]. Increasing the electrode potential to greater than +0.60 V changes the impedance from negative to positive and decreases the diameter of the arcs, indicating faster electron-transfer kinetics at higher potentials; at these potentials, CO adsorbed on the Pt surface was completely removed such that the surface reaction sites occupied by CO were recovered, leading to the diminishment of charge-transfer resistance.

For ethanol oxidation on the Pd$_4$Au/C and Pd$_{2.5}$Sn/C electrodes, it is evident that the impedance profiles (panels B and C) are quite different from those on Pt/C. All the impedance spectra obtained on both PdAu/GC and PdSn/GC electrodes are located within the first quadrant, and the arc diameters decrease with increasing potential. As expected, Pd and Pd alloys exhibit much better tolerance to CO poisoning than Pt, which was reflected by the absence of negative impedance for the PdAu/C and PdSn/C electrodes. It should also be
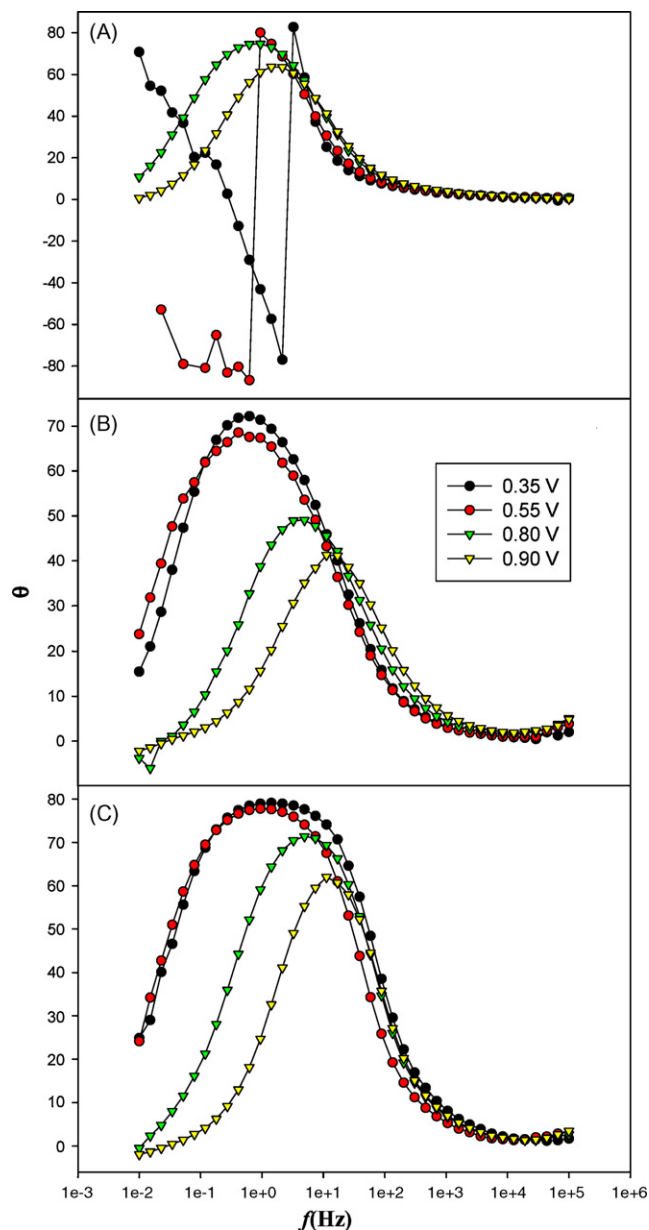
noted that the diameters of the impedance arcs of the Pt/C electrode are somewhat smaller than those on Pd$_4$Au/C and Pd$_{2.5}$Sn/C, suggesting faster electron-transfer kinetics on Pt than that on the Pd alloy particles. The impedance results agree well with the voltammetric results presented above.

Fig. 7 depicts the corresponding Bode plots of ethanol oxidation on the Pt/C, Pd$_4$Au/C, and Pd$_{2.5}$Sn/C electrodes. It can be seen that there is a maximum phase angle at a characteristic frequency (f) for all the electrodes. The characteristic frequency clearly increases with increasing potential, suggesting the corresponding electrochemical reaction rate increases with potential, as f usually represents the time constant of an electrochemical reaction [46,50]. It should be noted that on Pt/C, at potentials lower than +0.60 V, there is an abrupt jump between the positive and negative phase angles, corresponding to the negative faradic impedance in the Nyquist plots shown in Fig. 6(A). This phenomenon may be attributed to the oxidation of adsorbed CO and the resulting
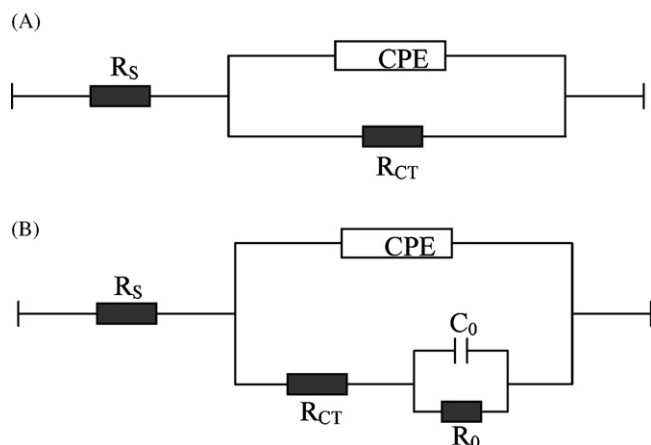
Fig. 8. Equivalent circuits for the electro-oxidation of ethanol: (A) for normal impedance, and (B) for negative impedance shown in Figs. 6 and 7.

inductive component of the Pt/C electrode. Again, for Pd$_4$Au/C and Pd$_{2.5}$Sn/C electrodes, no such behavior was observed due to minimal CO poisoning.

Based on the voltammetric and impedance results, the equivalent circuit shown in Fig. 8 was used to fit the EIS data. Fig. 8(A) depicts the equivalent circuit for the electrodes that exhibit normal impedance behaviors, where R_S represents the solution resistance, CPE (constant-phase element) is the double-layer capacitance, and R_{CT} is the charge-transfer resistance. For negative impedance observed on the Pt/C electrode, the equivalent circuit is shown in Fig. 8(B), where C_0 and R_0 represent the capacitance and resistance of the electrooxidation of adsorbed CO intermediates. The representative fits (solid lines) for the three electrodes are shown in each of the Nyquist plots in Fig. 6. From the fitting, the variation of the charge-transfer resistance (R_{CT}) with electrode potentials was evaluated, which was depicted in Fig. 9. First, negative R_{CT} was obtained on the Pt/C electrode at potentials lower than +0.55 V, due to the electrooxidation of surface-adsorbed CO species. Second, R_{CT} on all the three electrodes decreases with increasing electrode potential, indicating enhanced ethanol oxidation dynamics. Third, R_{CT} for ethanol oxidation on Pd$_{2.5}$Sn/C electrode is much larger than that on the Pt/C and Pd$_4$Au/C electrodes, suggesting that the electron-transfer kinetics at the Pd$_{2.5}$Sn/C electrode is the most sluggish among the three electrocatalysts. Overall, the impedance results
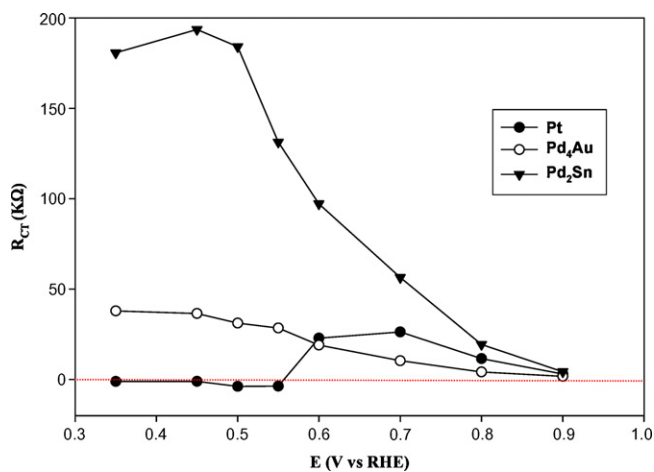
show that Pt/C exhibits heavy CO poisoning, Pd$_{2.5}$Sn/C shows low electrocatalytic activity for ethanol oxidation, and Pd$_4$Au/C displays the best catalytic activity because of its excellent CO-tolerance and fast reaction kinetics.

The different effects of Au and Sn on Pd/C catalytic performance remain unclear at this stage. A possible explanation is that Au and Sn behave as bi-functional elements similar to what Ru does to Pt/C in methanol oxidation [21,51,52]. It is well known that gold is a good catalyst for CO [4,53,54] and methanol oxidation [55,56]. In the case of Sn, an oxide layer may be formed in the high pH environment that compromises its catalytic activity.

4. Conclusions

This study demonstrates the feasibility of replacing Pt/C with Pd$_4$Au/C and Pd$_{2.5}$Sn/C as effective catalysts for the direct electrooxidation of ethanol in high pH media. XRD results show that Pd$_4$Au/C and Pd$_{2.5}$Sn/C belong to different space groups and have appreciable differences in crystal structure. The average particle size of as synthesized Pd$_4$Au/C and Pd$_{2.5}$Sn/C catalysts are 6.8 and 8.4 nm, respectively, as determined from XRD and TEM measurements. Although Pt/C shows better kinetics for ethanol oxidation as manifested by the more negative onset potential and larger instantaneous current density, Pd$_4$Au/C and Pd$_{2.5}$Sn/C are more tolerant to poisoning as shown in chronoamperometric tests. In impedance studies, Pt/C exhibits heavy CO poisoning and Pd$_{2.5}$Sn/C shows low electrocatalytic activity for ethanol oxidation. Pd$_4$Au/C displays the best catalytic activity among the three for ethanol direct oxidation in alkaline media.

Fig. 9. Charge-transfer resistance (R_{CT}) of ethanol electro-oxidation at different electrode potentials on Pt/C, Pd$_4$Au/C, and Pd$_{2.5}$Sn/C electrodes (shown as figure legends). Data are obtained by curve fitting of the impedance spectra (Figs. 6 and 7) using the equivalent circuits in Fig. 8.

References

[1] J.R. Varcoe, R.C.T. Slade, Fuel Cells 5 (2) (2005) 187–200.
[2] J.R. Varcoe, R.C.T. Slade, Solid State Ionics 176 (5–6) (2005) 585–597.
[3] C. Xu, P. Shen, X. Ji, R. Zeng, Y. Liu, Electrochem. Commun. 7 (2005) 1305–1308.
[4] F.J. Rodriguez Varela, O. Savadogo, J. Electrochem. Soc. 155 (6) (2008) B618–B624.
[5] A. Oliveira Neto, L.A. Farias, R.R. Dias, M. Brandalise, M. Linardi, E.V. Spinace, Electrochem. Commun. 10 (9) (2008) 1315–1317.
[6] A. Bonesi, G. Garaventa, W.E. Triaca, A.M. Castro Luna, Int. J. Hydrogen Energy 33 (13) (2008) 3499–3501.
[7] D.J. Berger, Science 286 (5437) (1999) 49.
[8] P. Shen, C. Xu, Electrochem. Commun. 8 (2006) 184–188.
[9] C. Xu, L. Cheng, P. Shen, Y. Liu, Electrochem. Commun. 9 (2007) 997–1001.
[10] C. Xu, P. Shen, Y. Liu, J. Power Sources 164 (2007) 527–531.
[11] F. Hu, F. Ding, S. Song, P. Shen, J. Power Sources 163 (2006) 415–419.
[12] H. Wang, C. Xu, F. Cheng, S. Jiang, Electrochem. Commun. 9 (2007) 1212–1216.
[13] C. Xu, H. Wang, P. Shen, S. Jiang, Adv. Mater. 19 (2007) 4256–4259.
[14] C. Xu, Y. Liu, D. Yuan, Int. J. Electrochem. Sci. 2 (2007) 674–680.
[15] H. Zheng, Y. Li, S. Chen, P. Shen, J. Power Sources 163 (2006) 371–375.
[16] J. Liu, J. Ye, C. Xu, S. Jiang, Y. Tong, Electrochem. Commun. 9 (2007) 2334–2339.
[17] C. Xu, Z. Tian, P. Shen, S.P. Jiang, Electrochim. Acta 53 (2008) 2610–2618.
[18] C. Xu, Z. Tian, Z. Chen, S. Jiang, Electrochem. Commun. 10 (2008) 246–249.
[19] F. Hu, C. Chen, Z. Wang, G. Wei, P.K. Shen, Electrochim. Acta 52 (2006) 1087–1091.
[20] C. Roth, N. Benker, R. Theissmann, R.J. Nichols, D.J. Schiffrin, Langmuir 24 (5) (2008) 2191–2199.
[21] Z.D. Wei, L.L. Li, Y.H. Luo, C. Yan, C.X. Sun, G.Z. Yin, P.K. Shen, J. Phys. Chem. B 110 (51) (2006) 26055–26061.
[22] Z. Jusys, T.J. Schmidt, L. Dubau, K. Lasch, L. Jörissen, J. Garche, R.J. Behm, J. Power Sources 105 (2) (2002) 297–304.
[23] J. Mann, N. Yao, A.B. Bocarsly, Langmuir 22 (25) (2006) 10432–10436.
[24] E. Herrero, K. Franaszczuk, A. Wieckowski, J. Phys. Chem. B 98 (1994) 5074–5083.
[25] B.D. Cullity, S.R. Stock, Elements of X-ray Diffraction, 3rd ed., Prentice Hall, Upper Saddle River, NJ, 2001.
[26] H. Li, G. Sun, L. Cao, L. Jiang, Q. Xin, Electrochim. Acta 52 (2007) 6622–6629.

[27] V. Rao, C. Cremers, U. Stimming, L. Cao, S. Sun, S. Yan, G. Sun, Q. Xin, J. Electrochem. Soc. 154 (11) (2007) B1138–B1147.
[28] M. Umeda, H. Sugii, I. Uchida, J. Power Sources 179 (2008) 489–496.
[29] P. Shen, C. Xu, R. Zeng, Y. Liu, Electrochem. Solid-State Lett. 9 (2) (2006) A39–A42.
[30] F.C. Simoes, D.M. dos Anjos, F. Vigier, J.-M. Leger, F. Hahn, C. Coutanceau, E.R. Gonzalez, G. Tremiliosi-Filho, A.R. de Andrade, P. Olivi, K.B. Kokoh, J. Power Sources 167 (1) (2007) 1–10.
[31] H. Wang, Z. Jusys, R.J. Behm, J. Power Sources 154 (2006) 351–359.
[32] J. Ribeiro, D.M. Anjos, J.-M. Leger, F. Hahn, P. Olivi, A.R. Andrade, G. Tremiliosi-Filho, K.B. Kokoh, J. Appl. Electrochem. 38 (5) (2008) 653–662.
[33] Q. Wang, G. Sun, L. Jiang, M. Zhu, G. Wang, Q. Xin, S. Sun, C. Chen, Y. Jiang, S. Chen, Guangpuxue Yu Guangpu Fenxi 28 (1) (2008) 47–50.
[34] E. Antolini, J. Power Sources 170 (2007) 1–12.
[35] F. Vigier, C. Coutanceau, F. Hahn, E.M. Belgsir, C. Lamy, J. Electroanal. Chem. 563 (2004) 81–89.
[36] H. Pang, J. Chen, L. Yang, B. Liu, X. Zhong, X. Wei, J. Solid State Electrochem. 12 (3) (2008) 237–243.
[37] S.A. Kirillov, P.E. Tsiakaras, I.V. Romanova, J. Mol. Struct. 651–653 (2003) 365–370.
[38] A. Schwartz, L.L. Holbrook, H. Wise, J. Catal. 21 (1971) 199–207.
[39] H. Gabasch, E. Kleimenov, D. Teschner, S. Zafeiratos, M. Hävecker, A. Knop-Gericke, R. Schlögl, D. Zemlyanov, B. Aszalos-Kiss, K. Hayek, B. Klötzer, J. Catal. 242 (2006) 340–348.
[40] J. Mizsei, J. Voutilainen, S. Saukko, V. Lantto, Thin Solid Films 391 (2001) 209–215.
[41] H.L. Tidahy, S. Siffert, F. Wyrwalski, J.-F. Lamonier, A. Aboukaïs, Catal. Today 119 (1–4) (2007) 317–320.
[42] K. Okumura, T. Kobayashi, H. Tanaka, M. Niwa, Appl. Catal. B 44 (4) (2003) 325–331.
[43] N.T.S. Phan, M. Van Der Sluys, C.W. Jones, Adv. Synth. Catal. 348 (6) (2006) 609–679.
[44] G. Wu, L. Li, B. Xu, Electrochim. Acta 50 (2004) 1–10.
[45] P. Bommersbach, M. Mohamedi, D. Guay, J. Electrochem. Soc. 154 (8) (2007) B876–B882.
[46] I.M. Hsing, X. Wang, Y.J. Leng, J. Electrochem. Soc. 149 (5) (2002) A615–a621.
[47] A.C. Chen, D.J. La Russa, B. Miller, Langmuir 20 (22) (2004) 9695–9702.
[48] W. Chen, J.M. Kim, S.H. Sun, S.W. Chen, Langmuir 23 (22) (2007) 11303–11310.
[49] W. Chen, J.M. Kim, L.P. Xu, S.H. Sun, S.W. Chen, J. Phys. Chem. C 111 (36) (2007) 13452–13459.
[50] W. Sugimoto, K. Aoyama, T. Kawaguchi, Y. Murakami, Y. Takasu, J. Electroanal. Chem. 576 (2) (2005) 215–221.
[51] P. Waszczuk, J. Solla-Gullón, H.-S. Kim, Y.Y. Tong, V. Montiel, A. Aldaz, A. Wieckowski, J. Catal. 203 (1) (2001) 1–6.
[52] T. Yajima, N. Wakabayashi, H. Uchida, M. Watanabe, Chem. Commun. (2003) 828–829.
[53] K. Mallick, M.S. Scurrell, Appl. Catal. A 253 (2) (2003) 527–536.
[54] M.M. Schubert, S. Hackenberg, A.C.V. Veen, M. Muhler, V. Plzak, R.J. Behm, J. Catal. 197 (1) (2001) 113–122.
[55] K.A. Assiongbon, D. Roy, Surf. Sci. 594 (1–3) (2005) 99–119.
[56] K. Miyazaki, K. Matsuoka, Y. Iriyama, T. Abe, Z. Ogumi, J. Electrochem. Soc. 152 (9) (2005) A1870–A1873.